Correction: 5 August 2021; see below

science.sciencemag.org/content/371/6532/eabb1625/suppl/DC1

Supplementary Materials for

Liver homeostasis is maintained by midlobular zone 2 hepatocytes

Yonglong Wei, Yunguan G. Wang, Yuemeng Jia, Lin Li, Jung Yoon, Shuyuan Zhang, Zixi Wang, Yu Zhang, Min Zhu, Tripti Sharma, Yu-Hsuan Lin, Meng-Hsiung Hsieh, Jeffrey H. Albrecht, Phuong T. Le, Clifford J. Rosen, Tao Wang, Hao Zhu*

*Corresponding author. Email: hao.zhu@utsouthwestern.edu

Published 26 February 2021, *Science* **371**, eabb1625 (2021)
DOI: 10.1126/science.abb1625

This PDF file includes:

Other Supplementary Material for this manuscript includes the following:
(available at science.sciencemag.org/content/371/6532/eabb1625/suppl/DC1)

MDAR Reproducibility Checklist (.pdf)
Tables S1 to S4 (.xlsx)

Correction: Several panels in fig. S2 were showing images from the same mouse rather than independent mice; these panels have been replaced with images from independent mice. Because expression patterns from independent mice are similar, the corrected figure does not substantially change the appearance of the images nor does it change the conclusions drawn from this figure.

Materials and methods

Generation of *CreER* knock-in lines. *IRES* was amplified from *MSCV-IRES-GFP* (Addgene #20672) and inserted into *pCAG-CreERT2* (Addgene #14797) using SacII/EcoRI. *IRES-CreERT2* flanked by homology arms from targeted genes were integrated into either *pUC19* or *pBluescriptSK(+)*. After sequencing, these plasmids were either directly injected with Cas9 mRNA and sgRNA into mouse zygotes, or used as templates to make double (ds) or single stranded (ss)DNAs, which were then co-injected with CAS9 protein and sgRNA(s). Different homology directed repair (HDR) constructs involving either ssDNA, linearized dsDNA, or circular plasmid DNA were used with varying success rates. All F0 mice were genotyped by a general *Cre* primer set and two pairs of knock-in specific primers that span the junction of a homology arm and the genomic DNA. PCR products produced with strain specific primers were cloned into the *pCR Blunt II-TOPO* vector (*Zero Blunt™ TOPO™*, Invitrogen) for sequencing.

Mouse strains, husbandry, and experimental methods. Mice were handled in accordance with the guidelines of the Institutional Animal Care and Use Committee at UTSW. All experiments were done in an age and sex controlled fashion unless otherwise noted. *Krt19-CreER* (*16*), *Axin2-CreER* (*33*, *34*), and *Sox9-CreER* (*35*) were obtained from Jackson Labs. Tamoxifen (Sigma-Aldrich) was dissolved in corn oil and subcutaneously (SC) injected into adult mice at doses indicated in Fig. S2B. Mice were maintained in the same pathogen free mouse facility under the same feeding, temperature, sterility conditions, which allowed us to compare results between tracing strains. All *CreER* mice were backcrossed onto the C57Bl6/J strain 2-3 times. The same sources of tamoxifen, CCl_4, and DDC were used. 5-10 male and 5-10 female mice were used in all experiments. For CRISPR screening, *Fah* KO mice were originally obtained from Yecuris Lab and maintained on the C57Bl6/J strain background. *Fah* KO mice were provided 7.5 μg/mL nitisinone water (Yecuris). For AAV experiments, mice were retro-orbitally injected with either control AAV-TBG-GFP or AAV-TBG-Cre ($5x10^8$ genome copies per mouse for low dose lineage tracing and $5x10^{10}$ genome copies per mouse for whole liver deletion in the case of *Ccnd1* floxed mice) at 6 months of age. For in vivo overexpression experiments, human *Igfbp2* was cloned into the pT3-EF1a plasmid and injected via HDT into wild-type mice. 48 hours later, livers were harvested.

Histology, immunohistochemistry, and immunofluorescence. For frozen sectioning, livers were fixed in 4% paraformaldehyde (PFA) then dehydrated in 30% sucrose in PBS. 16 μm thick sections were cut and washed with PBST 3x and blocked in 5% BSA + 0.25% Triton X-100. GS antibody (Abcam ab49873) in blocking buffer was incubated overnight. For H&E staining, livers were fixed in 10% neutral buffered formalin then incubated in 70% ethanol. Tissue was embedded, paraffin sectioned, and stained by the UTSW Histology Core. Immunohistochemistry was performed as previously described (*36*) with anti-CCND1 (Abcam ab16663), anti-IGFBP2 (Abcam ab188200) and anti-Ki-67 (Abcam ab15580). Whole slides were imaged using an Axioscan slide scanner and processed using Zen 2.6 software from Zeiss. To quantify the percent Tomato positive area, we used ImageJ. We first separated the composite RBG image (see the *Arg1.2-CreER* image below

as an example, panel A) into three channels: red (B), green (C) and blue (D). We first adjusted the threshold of the red channel to saturate all Tomato signals so that we could measure the percent of the image that was Tomato positive. In the below panel E, it is 72.6%. We then adjusted the threshold of the green channel such that we could exclude empty spaces such as vascular lumens and regions of the image not covered by cells. This allowed us to obtain the percent of the image that was actually covered by liver tissues. In the below panel F, it is 93.29%. We then divided the Tomato positive area by the total area occupied by tissue and obtained the actual percent Tomato coverage (72.6%/93.3% = 77.8%).

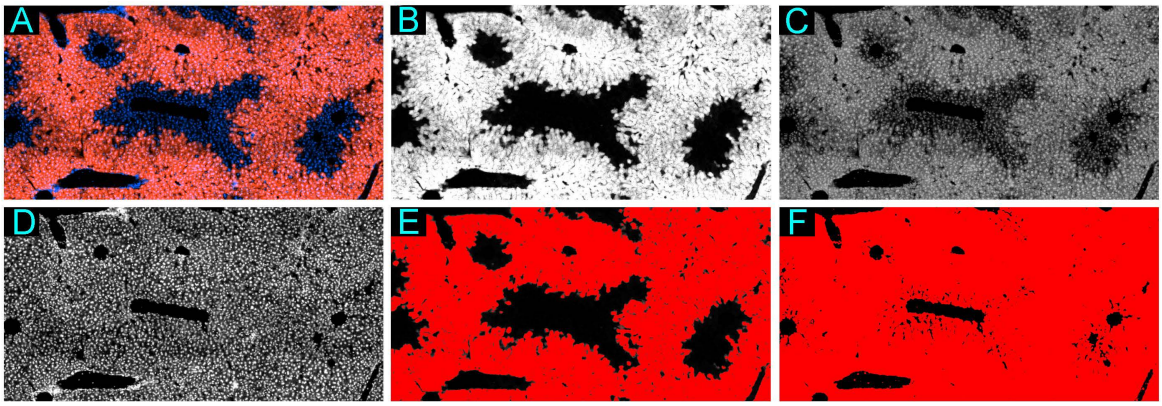

Chemical injury experiments. CCl_4 was injected IP at a dose of 2 µl/g of mouse weekly. DDC (Sigma-Aldrich) was integrated into LabDiet chow (#5015) at a 0.1% concentration. CCl_4 and DDC were provided for 6 weeks starting 2 weeks after tamoxifen.

Proliferation assays and quantification of zonal location. 10 days after tamoxifen, water containing 1 mg/ml EdU (Carbosynth, NE08701) was provided for 7-15 days depending on the experiment. EdU signal was detected in frozen sections using the Click-iT EDU Alexa Fluor 488 Imaging Kit (Life Technologies, C10337) following the manufacturer's instructions. GS and a fluorescent secondary antibody (Thermo Fisher, A-21245) were used to mark CVs. Zonation of EdU positive nuclei were quantified as follows. The position index (P.I.) was determined by the distance to the closest CV (x), the distance to the closest PV (y), and the distance between the CV and PV (z), based on the law of cosines. P.I. = $(x^2 + z^2 - y^2)/(2z^2)$. The same formula was used in Lin *et al* (*4*).

Clone size and clone number quantification. We used cell numbers to define clone size. To quantify clone size, we lowered the threshold of the Tomato channel so that we could see clear cell boundaries. We used 8 representative images, each with an area of 1.61×10^6 μM^2, from 4 representative mice (2 large images from one liver section per mouse) for each time point. We counted the total number of clones from the 8 representative images. Because the images were of equal area, the clone numbers can be compared to each other between time points.

scRNA-seq data generation, processing, and clustering. Primary unsorted hepatocytes were isolated with a standard two-step collagenase perfusion method (*37*). Cells were washed and resuspended in hepatocyte washing medium (Life, 17704024). Flow cytometry

was used to quantify the frequency of Tomato positive cells, but the scRNA-seq was done on a separate batch of unsorted cells from the same livers. Single cell libraries were prepared using the 10x Genomics Chromium Single Cell 3' Reagents Kit v3. For each sample, 8,000 hepatocytes were loaded to target ~5,000 cells after recovery according to the manufacturer's protocol. Single cell libraries were generated and sequenced using the 150 bp paired-end Illumina NextSeq500 in the UT Southwestern Children's Research Institute Sequencing Facility. 10x scRNA-seq data was preprocessed using Cellranger v3.0.2 software. We used the "*mkfastq"* and "*count"* commands to process the 10x single-cell RNA-seq output into cells by gene expression count matrix, and used the "*aggr"* command to pool sequencing runs (https://github.com/10XGenomics/cellranger). All parameters were set to default except for the "force-cells" parameter, which was set to 4000. A custom constructed hybrid transcriptome reference combining the mouse transcriptome mm10 and the Ai9 plasmid sequence (Addgene #22799) was used to enable simultaneous calling of endogenous mouse mRNA and tdTomato expression. scRNA-seq data analysis was performed with the scanpy (1.4.4) package in Python (*38*). Cell and gene filtering were performed as follows: genes expressed in less than 3 cells and cells with a very small library size (<100) were removed. Cells with a very high (>= 0.5) mitochondrial genome transcript ratio were removed. For downstream analysis, we transformed the gene counts into log(CPM+1) values, where the total library size in each cell was used to normalize each gene's expression. After normalization, batch effects were removed using the Mutual Nearest Neighbor algorithm (*39*), and clustering was performed on batch effect normalized data using the Louvain clustering algorithm (*40*). Briefly, principal component analysis (PCA) was used to reduce the number of dimensions representing each cell (n_components = 50), then a weighted nearest neighbor graph was built from the PCA transformed data using the "*pp.neighbors"* function in the scanpy package. Finally, a partition of the graph that maximizes modularity was found with the Leiden algorithm (*40*), which is an improved version of the Louvain algorithm (*41*). We used the detection method using the "*tl.leiden"* function in the scanpy package. We excluded all ribosomal associated genes from the clustering analysis. The most highly expressed genes from each cluster were found using the "*tl.rank_genes_groups"* function in the scanpy package, which is based on the student's T-test between target and reference cell populations.

In vivo CRISPR screening. SgRNA sequences were obtained from either the Mouse GeCKO v2 library (Addgene #1000000052) or the Mouse Genome-wide CRISPRa-v2 Library (Addgene #83996). These were synthesized by Genewiz as an oligoarray and then cloned into CRISPR KO or CRISPRa library plasmids described previously (*25*). 5 µg of either of these plasmids and 2 µg of SB100 (Addgene #34879) were resuspended in 0.9% NaCl solution to a final volume of 10% of mouse body weight, and hydrodynamically transfected (HDT) into 8-10 week old *Fah* KO mice through the tail vein. Nitisinone water was withdrawn immediately after HDT. One month later, livers were collected, snap frozen in liquid nitrogen, and made into a powder using a mortar and pestle. Half of the tissue was suspended in digestion buffer (100 mM NaCl, 10 mM Tris-Cl (pH 8.0), 25 mM EDTA (pH 8.0), 0.5% SDS, and 0.1 mg/mL proteinase K) and digested overnight at 50°C. After digestion, 0.1% SDS and 1 ug/ml DNase-free Rnase was added and incubated for 1 hour at 37°C to remove residual RNA. Genomic DNA extraction of 1 mL of digested tissue was performed with an equal volume of phenol/chloroform/isoamyl alcohol (25:24:1), followed

by ethanol precipitation. The DNA concentration was determined with the Qubit dsDNA BR assay kit. PCR amplicon libraries for deep sequencing were made using methods from (*42*). The transposon library used for the HDT injection was sequenced as a control. The library was prepared to ensure 1000-fold coverage. All samples were sequenced on an Illumina HiSeq500 with 75 bp single-end reads. ~1-2 million reads were sequenced per library.

To see if the screens could identify genes that are potentially necessary and sufficient for hepatocyte proliferation, we used looser criteria for identifying genes. Because in vivo screens have lower coverage for individual sgRNAs, we used less stringent criteria to nominate genes, then we use validation to confirm hits near the top of the screen list. For the CRISPR KO screen we used a p-value cutoff of < 0.15, which included *Ahctf1* ($p = 0.001$), *Ccnd1* ($p = 0.005$), and *Hamp2* ($p = 0.054$). For the CRISPRa screen we also used a p-value cutoff of < 0.15, which included *Ahctf1* ($p = 0.099$), *Ccnd1* ($p = 0.118$), and *Hamp2* ($p = 0.123$). See Table S4 for details. Looser cutoffs allowed us to identify shared hits between both screens.

Western Blot Analysis. Mouse liver tissues were ground and lysed in protein lysis buffer and Western blots were performed. Antibodies used: anti-CCND1 (Abcam ab16663 or CST #55506), anti-β-Actin (CST #4970), anti-S6K (CST #2708), anti-pS6K (CST #9205), anti-IGFBP2 (Abcam ab188200), anti-Rb (Abcam ab181616), anti-p-Rb (CST #9307), anti-Akt (CST #9272), anti-p-Akt (CST #4060), anti-4E-BP1 (CST #9452), anti-p-4E-BP1 (CST #2855), anti-rabbit IgG, HRP-linked Antibody (CST #7074).

Drug treatments. INK128 (LC Biochem) was formulated in 5% polyvinyl propylene, 15% NMP and 80% water was given by oral gavage at 1 mg/kg daily for 12 days. Palbociclib was dissolved in sodium lactate buffer (50 mmol/L, pH 4.0) and administrated by oral gavage at 150 mg/kg daily for 12 days.

Statistical Analysis. The data in most panels reflect multiple experiments performed on different days using mice derived from different litters. Unless otherwise indicated in the figure legends, variation is always indicated using standard deviation presented as mean±SD. Unpaired Student's t-tests were used to test the significance of differences between groups. Statistical significance is displayed as $p<0.05$ (*), $p<0.01$ (**), $p<0.001$ (***). In all experiments, no mice were excluded from analysis after an experiment was initiated. Image analysis for the quantification was blinded.

Supplemental figures and captions

Fig. S1.

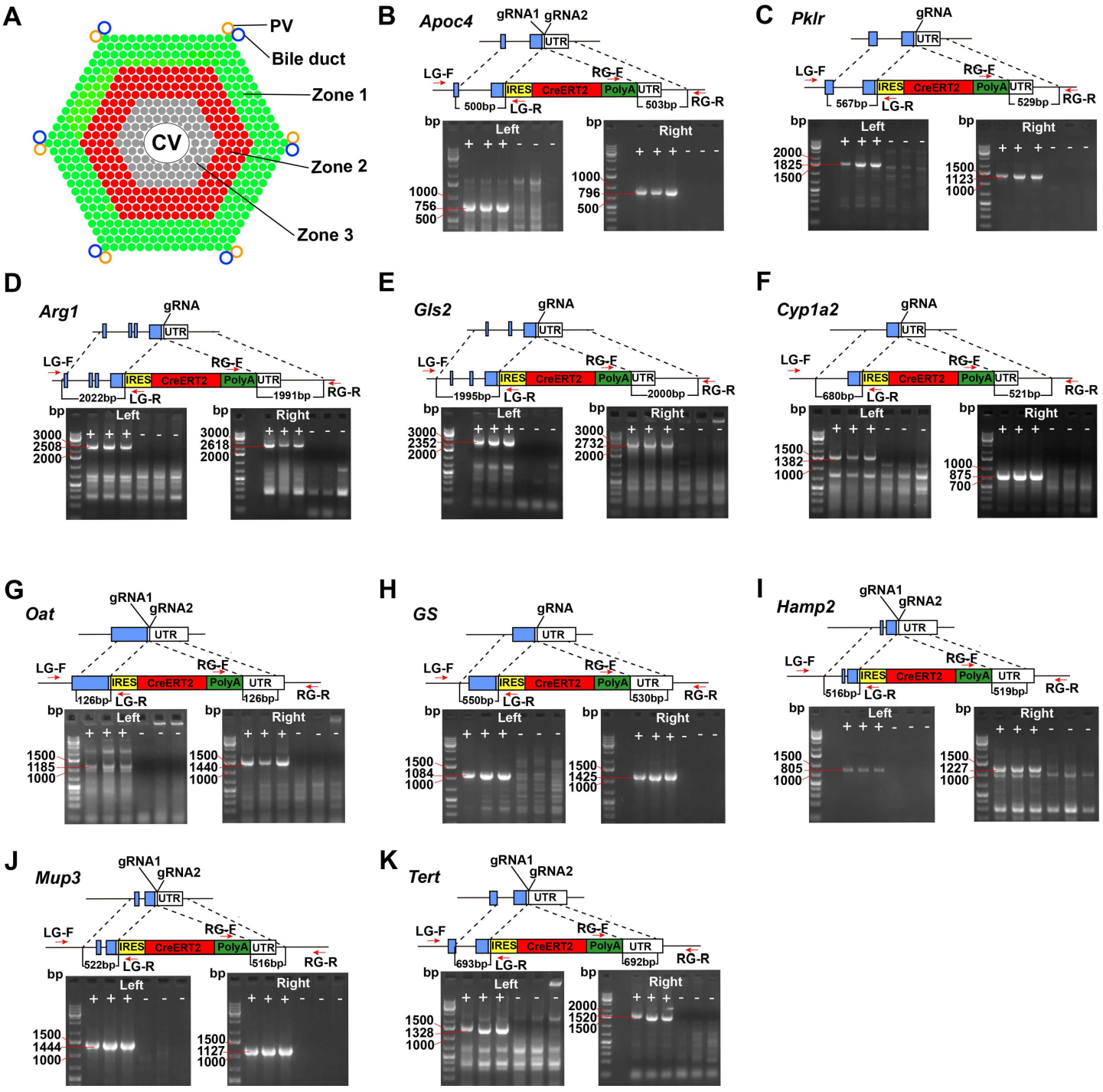

Fig. S1. Cartoon of the liver lobule and construct designs for all *CreER* knock-in mouse strains generated for this paper.

A. Cartoon of the liver lobule, which shows how zones are organized within a single lobule. Blood flows in the portal to the central direction.

B-K. Schema for the HDR constructs for each strain. Each HDR construct contains an *IRES-CreER-PolyA* tail. Shown are the original genomic loci and CRISPR edited loci. The sizes of the homology arms are shown. Expected PCR bands for left and right integration sites are shown. CRISPR targeting strategies and genotyping primers used are contained in Table S1.

Fig. S2.

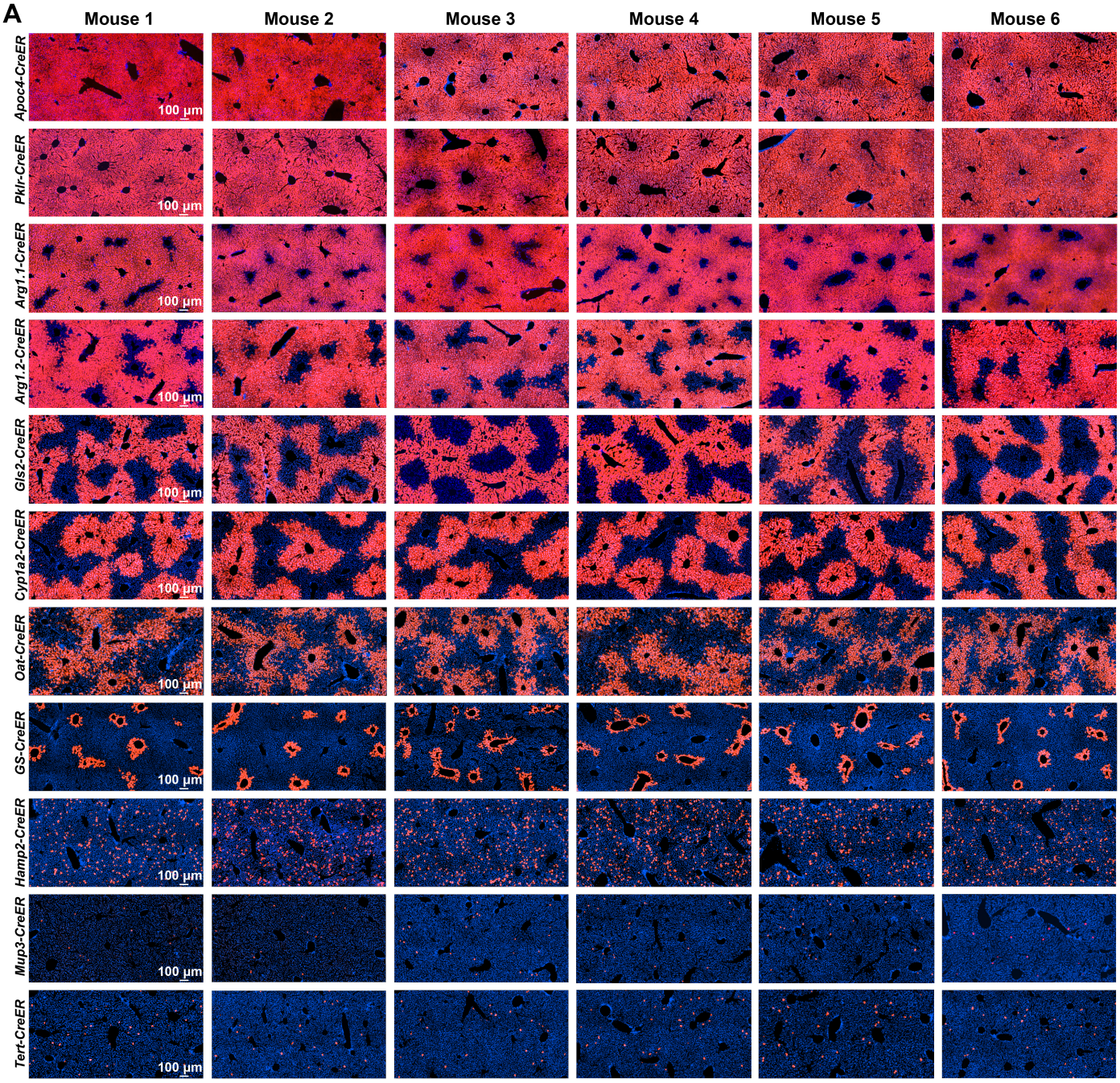

B

Line	*Apoc4*	*Arg1.1*	*Arg1.2*	*Axin2*	*Cyp1a2*	*Gls2*	*GS*	*Hamp2*	*Krt19*	*Mup3*	*Oat*	*Pklr*	*Sox9*	*Tert*
TAM dose	100 mg/kg x 3	100 mg/kg x 1	100mg/kg x 1	100 mg/kg x 1	100 mg/kg x 1	100 mg/kg x 1	No TAM	100 mg/kg x 1	100 mg/kg x 3	100 mg/kg x 1	100 mg/kg x 1	100 mg/kg x 3	100 mg/kg x 1	100 mg/kg x 5

Fig. S2. Tamoxifen induction of Tomato reporter labeling is consistent between individual mice.

A. Tomato labeling within individual *CreER* mice was consistent for the same doses of tamoxifen.

B. Table showing tamoxifen dosing regimens for each mouse line.

Fig. S3.

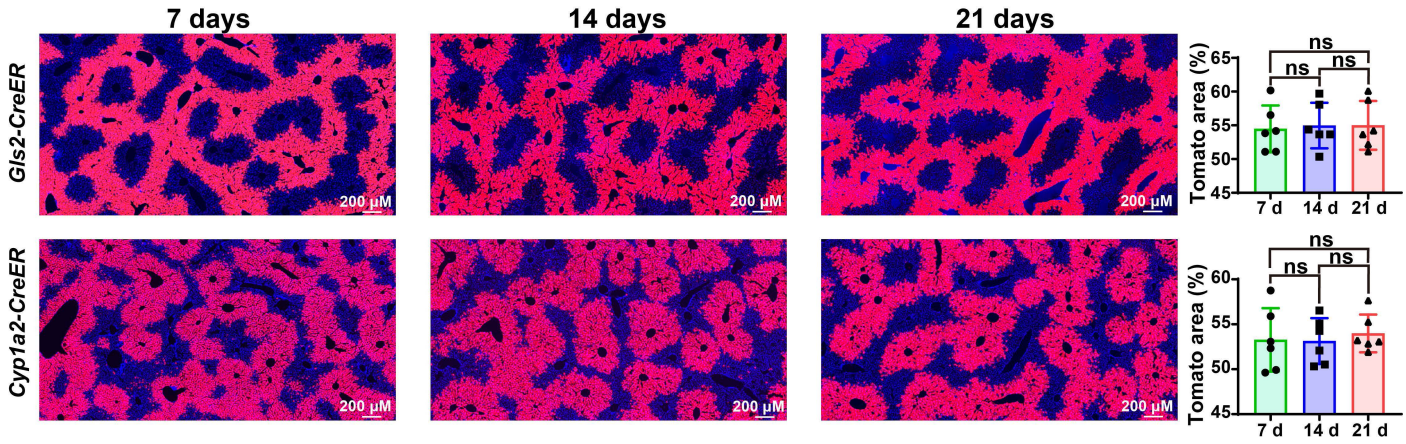

Fig. S3. Tomato labeling shows no significant changes between 7, 14, and 21 days after tamoxifen.

- **A.** Representative images of *Gls2-CreER* showing Tomato labeling 7, 14, and 21 days after tamoxifen administration. Quantification on the right.
- **B.** Representative images of *Cyp1a2-CreER* showing Tomato labeling 7, 14, and 21 days after tamoxifen administration. Quantification on the right.

Fig. S4.

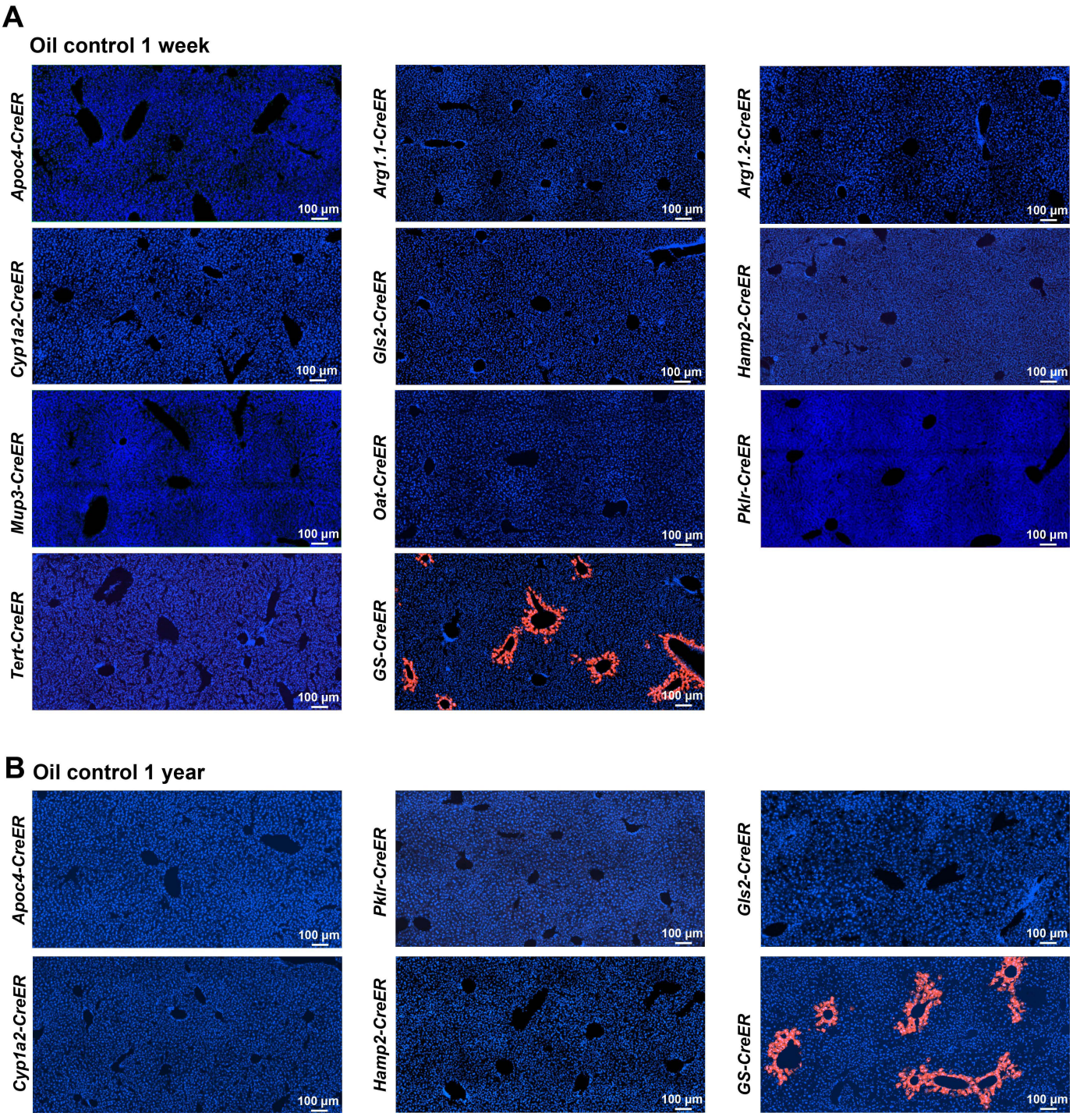

Fig. S4. Oil alone experiments to determine *CreER* leakiness.

A. 1 week after oil administration without tamoxifen, no Tomato staining was observed in these lines except for in *GS-CreER* mice.

B. 1 year after oil administration without tamoxifen, no Tomato staining was observed in these lines except for in *GS-CreER* mice.

Fig. S5.

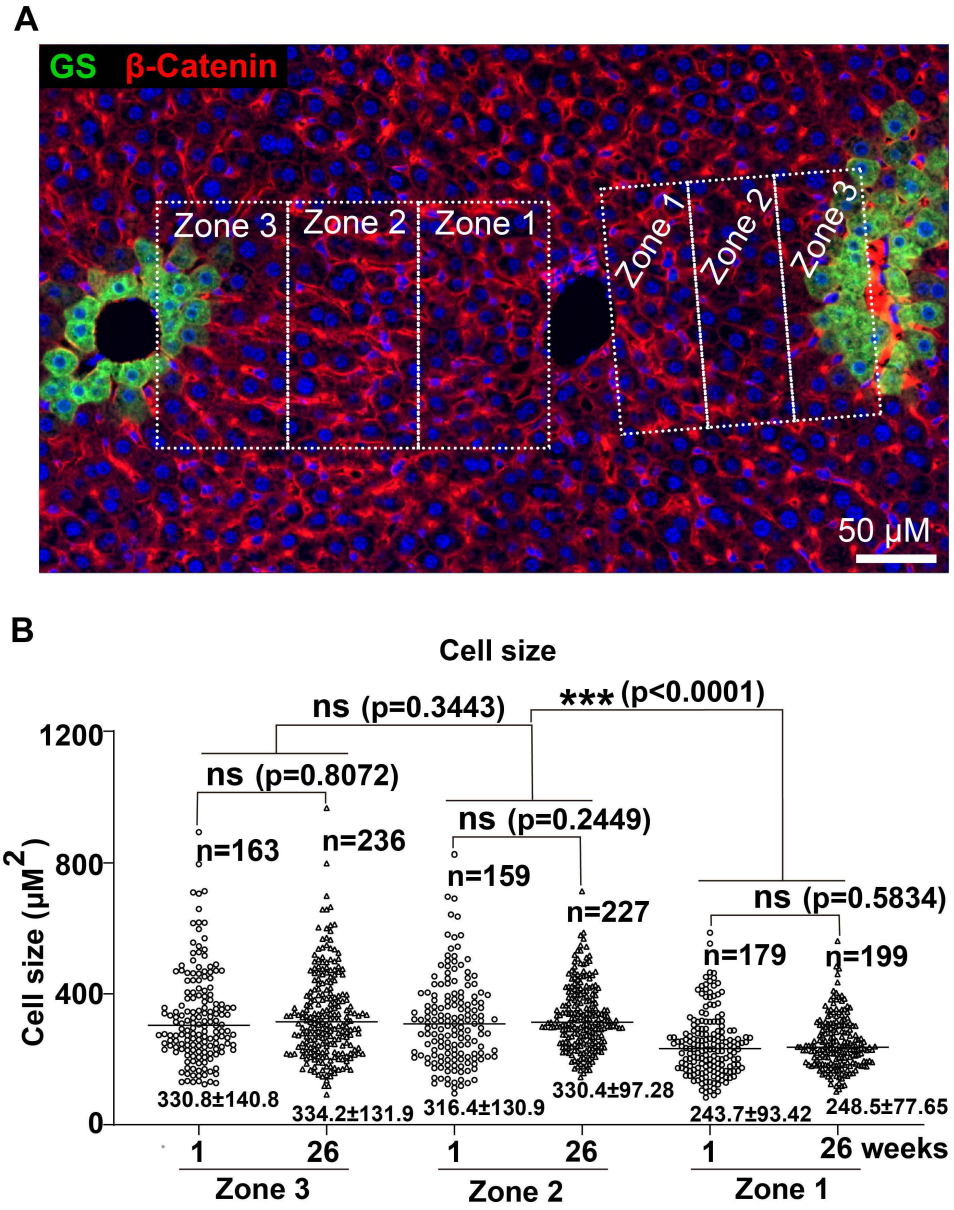

Fig. S5. Hepatocyte size as a function of zonal position and time.

A. Image showing a liver section IF stained with β-Catenin, GS, and DAPI. The cross-sectional areas occupied by individual hepatocytes were quantified in each zone.

B. Dot plots representing individual cell areas as a function of zone and time. Average area ±SD is written under each dot cluster. 6 images from 3 mice were measured.

Fig. S6.

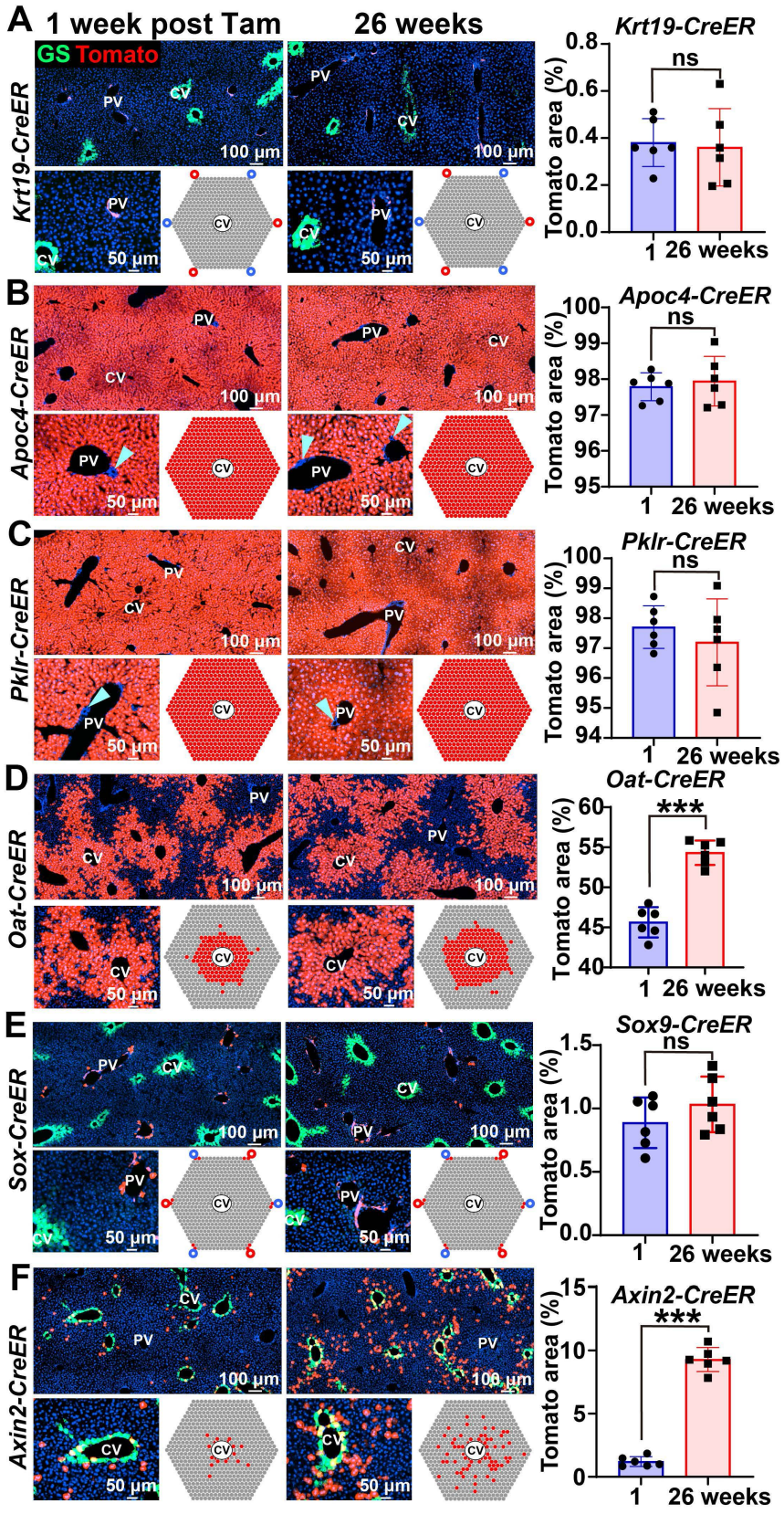
A
1 week post Tam
26 weeks
GS Tomato
Krt19-CreER
PV
CV
100 μm
50 μm
Krt19-CreER
Tomato area (%)
ns
1
26 weeks
B
Apoc4-CreER
Apoc4-CreER
C
Pklr-CreER
Pklr-CreER
D
Oat-CreER
Oat-CreER
***
E
Sox-CreER
Sox9-CreER
F
Axin2-CreER
Axin2-CreER
***

Fig. S6. Additional lineage tracing during 6 months of normal homeostasis.

- **A.** Over 6 months, the area labeled by *Krt19-CreER* was unchanged and remained within the biliary epithelial compartment. Note that there was no extension of Tomato labeling from the PV area into the lobule. Endogenous GS immunofluorescence is shown in green for all of the images in this figure.
- **B.** Over 6 months, the area labeled by *Apoc4-CreER* was unchanged and remained within the hepatocyte compartment. Note that there was no extension of Tomato labeling from the hepatocyte compartments into the bile duct (Arrowhead).
- **C.** Over 6 months, the area labeled by *Pklr-CreER* was unchanged and remained within the hepatocyte compartment. Note that there was no extension of Tomato labeling from the hepatocyte compartments into the bile duct (Arrowhead).
- **D.** Over 6 months, the area labeled by *Oat-CreER* increased in size from 46% to 53% coverage.
- **E.** Over 6 months, the area labeled by *Sox9-CreER* was unchanged. At 6 months, there was still labeling of hepatocytes near the PV.
- **F.** Over 6 months, the area labeled by *Axin2-CreER* increased from 2% to 10% coverage.

Fig. S7.

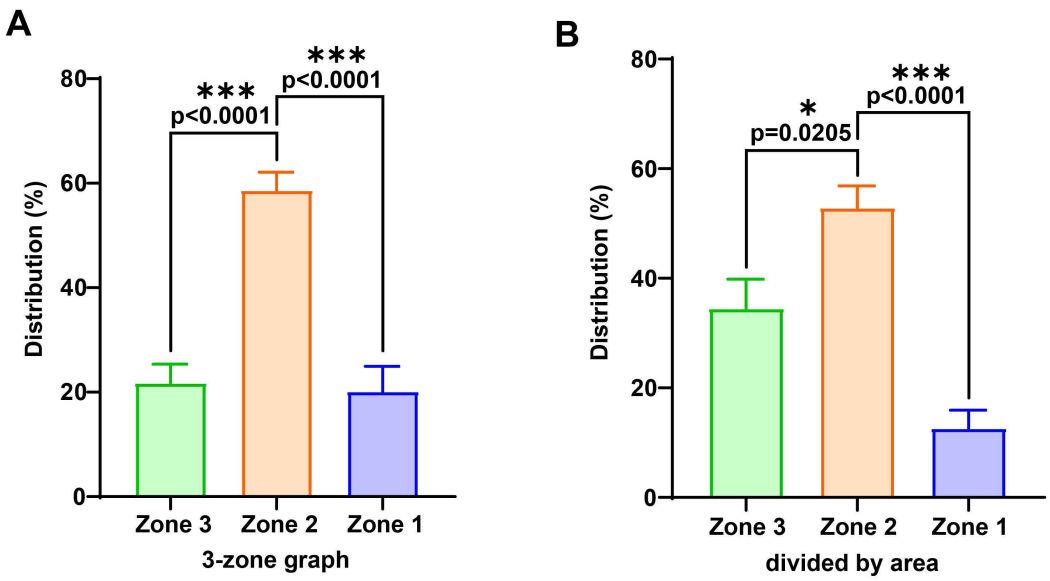

Fig. S7. EdU frequency as a function of zone, before and after normalization for zone size. When quantifying the number of proliferating cells in each zone, it is important to consider zone size. Here we used zone size as the denominator to normalize the number of proliferative cells based on lobular area. Based on area measurements for hexagons of different sizes, we have performed the normalization for all three zones. Even when we use this normalization, zone 2 still has the most proliferative cells.

- **A.** EdU positive cells in different zones without normalization by zone area.
- **B.** EdU positive cells in different zones with normalization by zone area. Error bars indicate standard error (SEM).

Fig. S8

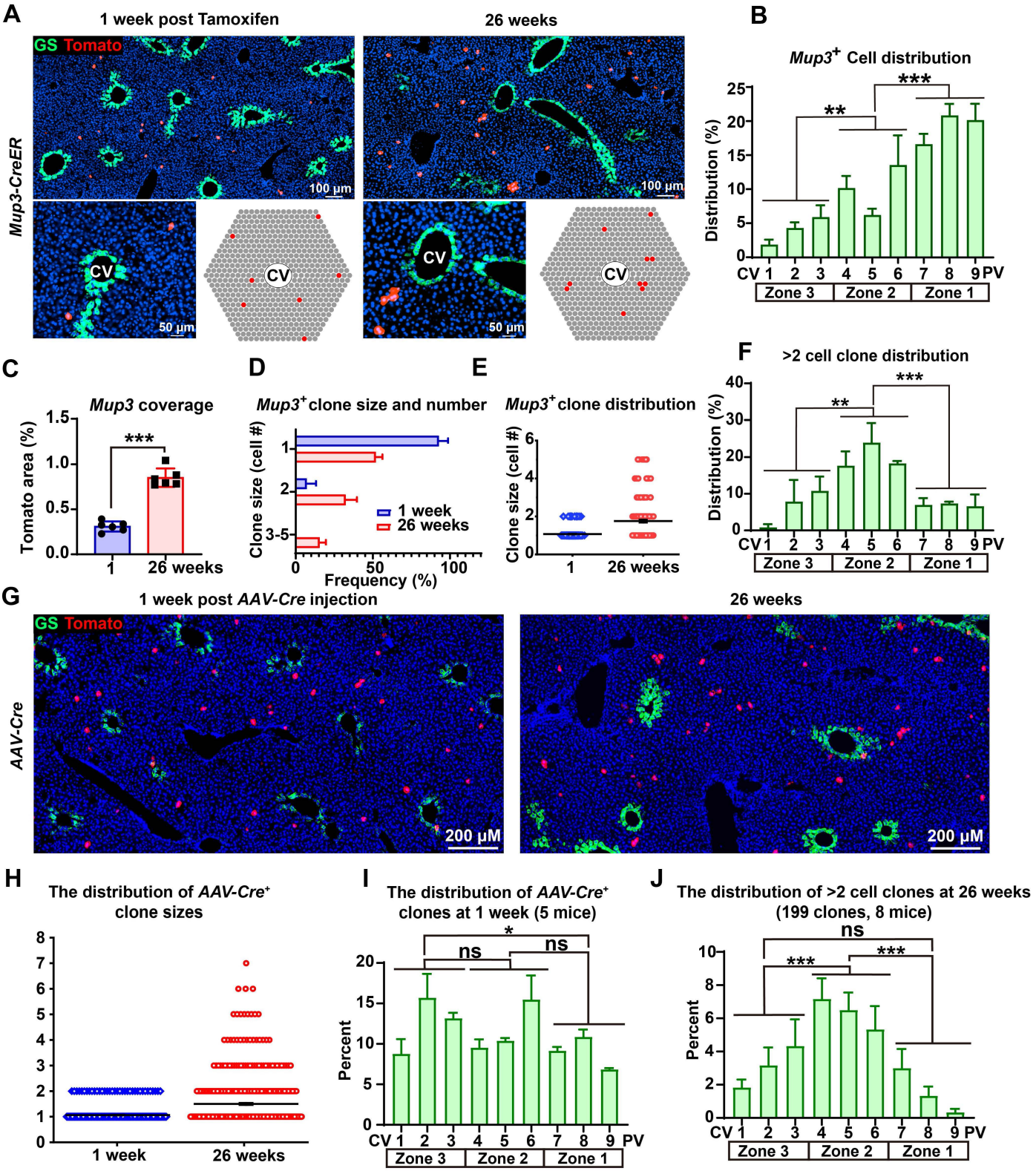
A
1 week post Tamoxifen
26 weeks
GS Tomato
Mup3-CreER
100 μm
50 μm
CV
B
Mup3+ Cell distribution
Distribution (%)
CV 1 2 3 4 5 6 7 8 9 PV
Zone 3
Zone 2
Zone 1
C
Mup3 coverage
Tomato area (%)
1
26 weeks
D
Mup3+ clone size and number
Clone size (cell #)
1 week
26 weeks
Frequency (%)
E
Mup3+ clone distribution
Clone size (cell #)
F
>2 cell clone distribution
G
1 week post AAV-Cre injection
26 weeks
AAV-Cre
200 μM
H
The distribution of AAV-Cre+ clone sizes
I
The distribution of AAV-Cre+ clones at 1 week (5 mice)
Percent
ns
J
The distribution of >2 cell clones at 26 weeks (199 clones, 8 mice)

Fig. S8. Clone size analysis of zone 2 hepatocytes labeled in *Mup3-CreER* mice and after AAV-TBG-Cre delivery.

- **A.** *Mup3-CreER* labeling at time 1 and 26 weeks. Endogenous GS immunofluorescence marks the CV region. Cartoon depicting pattern of Tomato labeling in *Mup3-CreER* livers over time (bottom right).
- **B.** Manual measurements of *Mup3-CreER* labeled Tomato positive cells as a function of position along the CV to PV axis.
- **C.** The percent area labeled by *Mup3-CreER* at 1 and 26 weeks after tamoxifen.
- **D.** Labeled clone size frequency in *Mup3-CreER* livers. Clone size increased modestly for most of the clones.
- **E.** Individual clone size distribution in *Mup3-CreER* livers.
- **F.** Manual measurements of CV to PV axis position for clones of >2 cells in *Mup3-CreER* mice 26 weeks after tamoxifen. This shows that most clonal growth was concentrated in zone 2.
- **G.** Representative images of Tomato mice injected with a low dose of AAV-TBG-Cre (100µl of $5x10^9$ viral genomes/mL) and traced for 1 or 26 weeks. Endogenous GS immunofluorescence marks the CV region.
- **H.** The size distribution of Tomato positive clones at 1 and 26 weeks after AAV-TBG-Cre administration.
- **I.** The spatial distribution of Tomato positive clones along the CV-PV axis 1 week after AAV-TBG-Cre administration. 100% of these clones were comprised of 1 or 2 cells.
- **J.** The spatial distribution of Tomato positive clones that were larger than 2 cells along the CV-PV axis 1 week after AAV-TBG-Cre administration. This distribution includes only the clones that underwent growth.

Error bars indicate SD except in S8B,F,I,J, where error bars indicate SEM.

Fig. S9.

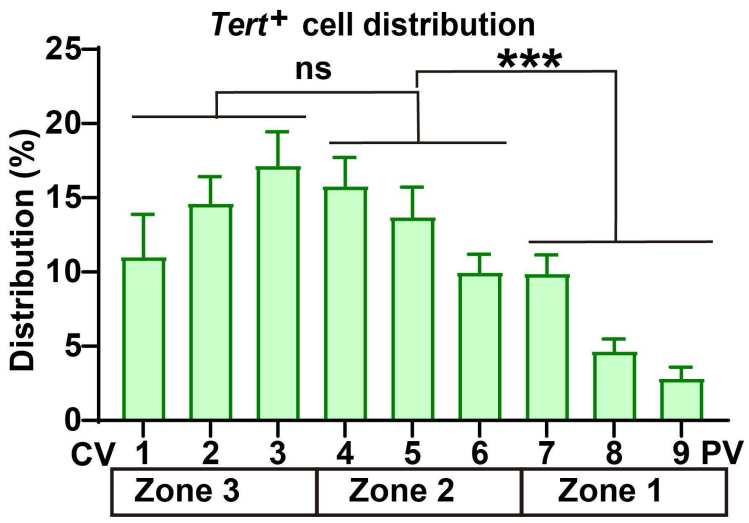

Fig. S9. Measurements of *Tert-CreER* labeled Tomato positive cells as a function of position along the CV to PV axis. Error bars here indicate SEM.

Fig. S10.

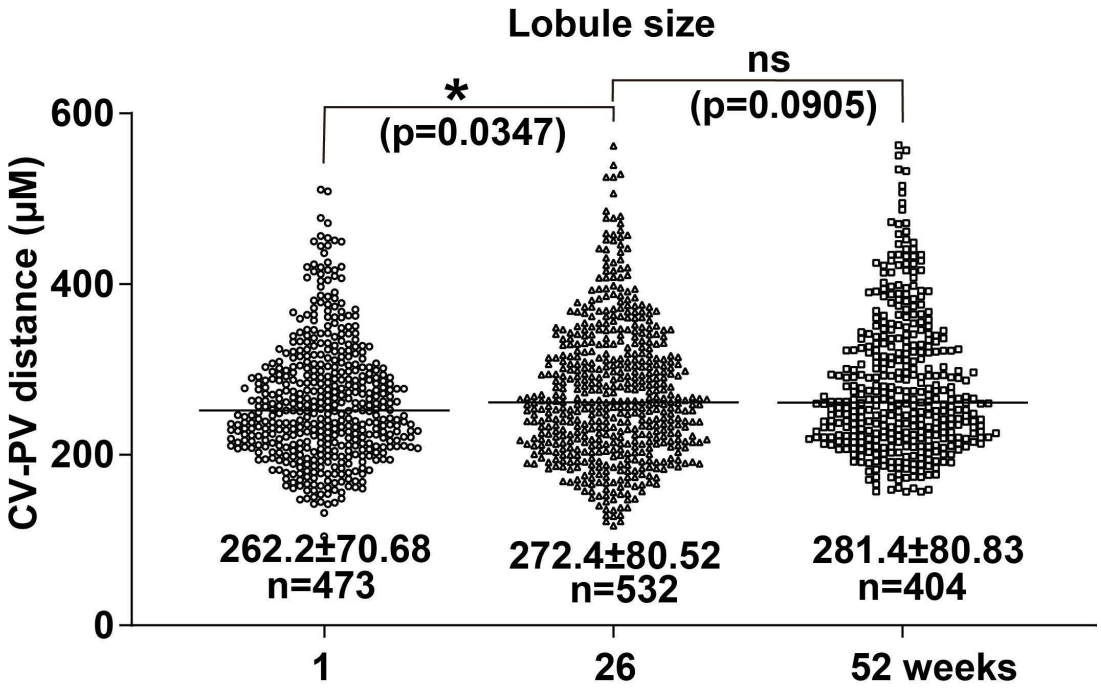

Fig. S10. Lobular size change over time as measured by CV to PV distances.

Fig. S11.

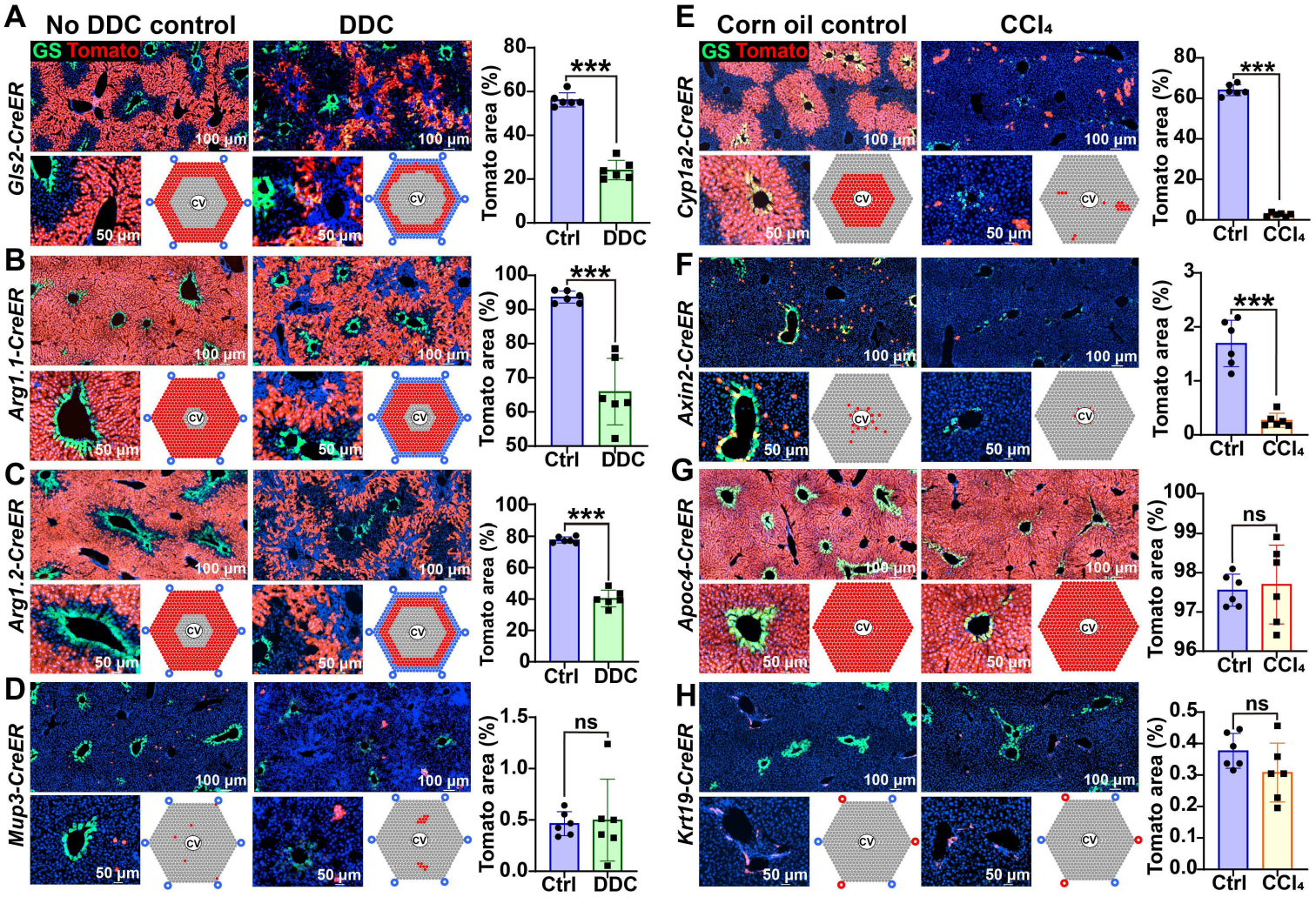

Fig. S11. Cellular contributions to regeneration after chronic periportal and centrilobular injuries. This data is associated with main Fig. 5.

- **A.** *Gls2-CreER* tracing after 6 weeks of DDC. Endogenous GS immunofluorescence marks the CV regions in all images of this figure.
- **B.** *Arg1.1-CreER* tracing after 6 weeks of DDC.
- **C.** *Arg1.2-CreER* tracing after 6 weeks of DDC
- **D.** *Mup3-CreER* tracing after 6 weeks of DDC.
- **E.** *Cyp1a2-CreER* tracing after 6 weeks of CCl_4.
- **F.** *Axin2-CreER* tracing after 6 weeks of CCl_4.
- **G.** *Apoc4-CreER* tracing after 6 weeks of CCl_4.
- **H.** *Krt19-CreER* tracing after 6 weeks of CCl_4.

Fig. S12.

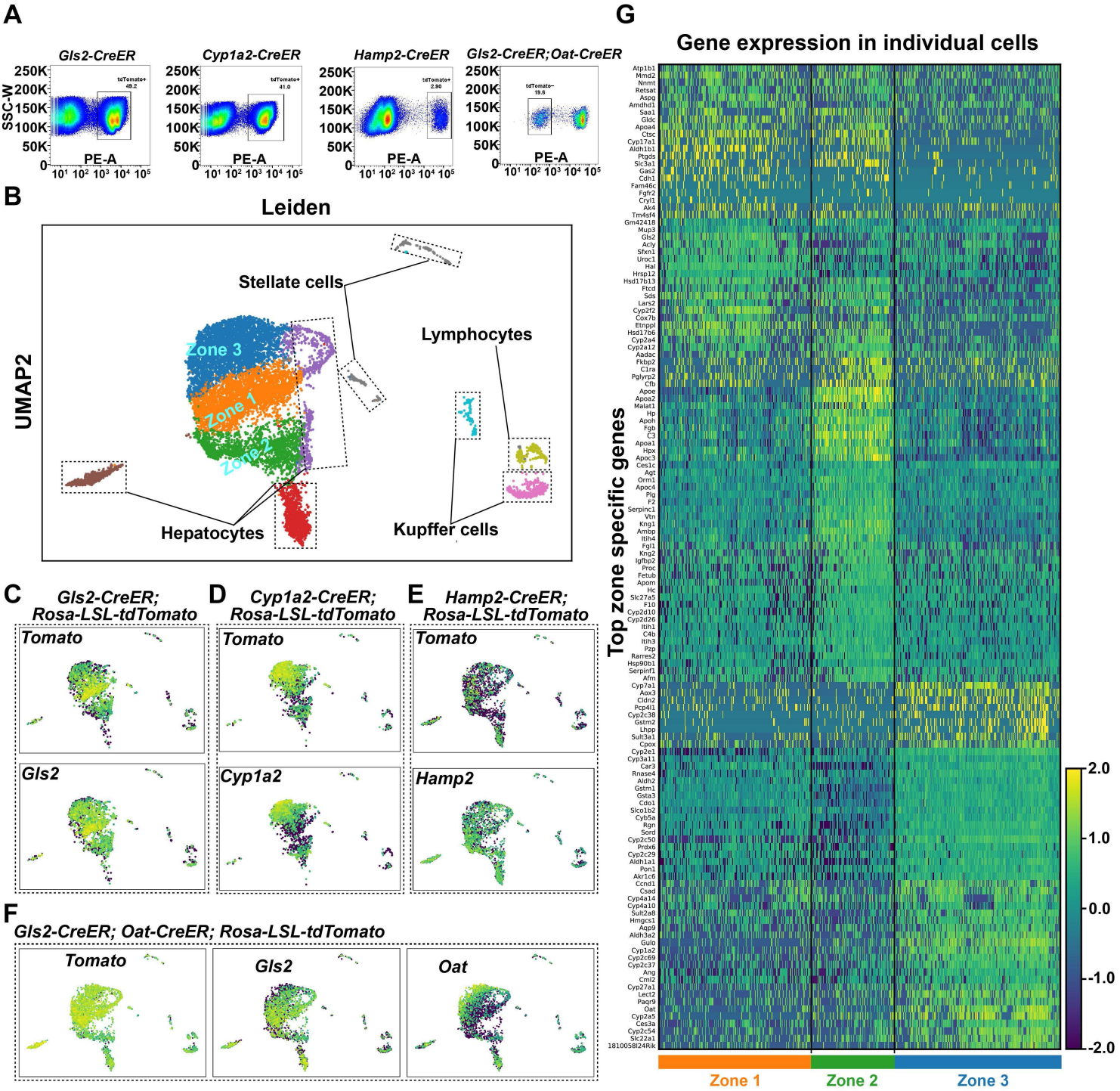
A
Gls2-CreER
Cyp1a2-CreER
Hamp2-CreER
Gls2-CreER;Oat-CreER
SSC-W
PE-A
B
Leiden
UMAP2
Stellate cells
Lymphocytes
Zone 3
Zone 1
Zone 2
Hepatocytes
Kupffer cells
C
Gls2-CreER; Rosa-LSL-tdTomato
D
Cyp1a2-CreER; Rosa-LSL-tdTomato
E
Hamp2-CreER; Rosa-LSL-tdTomato
Tomato
Gls2
Cyp1a2
Hamp2
F
Gls2-CreER; Oat-CreER; Rosa-LSL-tdTomato
Tomato
Gls2
Oat
G
Gene expression in individual cells
Top zone specific genes
Zone 1
Zone 2
Zone 3
2.0
1.0
0.0
-1.0
-2.0

Fig. S12. Characterization of zonal *CreER* mouse lines using scRNA-seq.

A. Flow analysis showed that Tomato positive cells in *Gls2-CreER*, *Cyp1a2-CreER* and *Hamp2- CreER* mouse livers account for 41%, 49% and 2.9% of the total live cell population, respectively. Tomato negative cells in *Gls2-CreER; Oat-CreER* mouse livers, which include zone 2 hepatocytes that are not labelled, account for 19.6% of total live cell population. Differences between fraction of cells labeled vs. image area quantifications could reflect differences in cell size. For example, hepatocytes are larger that biliary epithelia and blood cells, thus the same number of hepatocytes account for more area.

B. scRNA-seq UMAP plot of all four individual livers combined. This shows distinct cellular populations as identified by unsupervised clustering in uninjured livers. Different zone-specific genes are enriched in corresponding clusters.

C-F. scRNA-seq UMAP plots showing expression of Tomato and the endogenous genes in which *CreER* is knocked-in. The identity of the mouse is written above individual plots.

G. Heatmap shows the distribution of the top zone-specific genes in individual hepatocytes from zone 1, 2, or 3. Expression data values associated with this figure panel can be found in Table S2, Sheet 1.

Fig. S13.

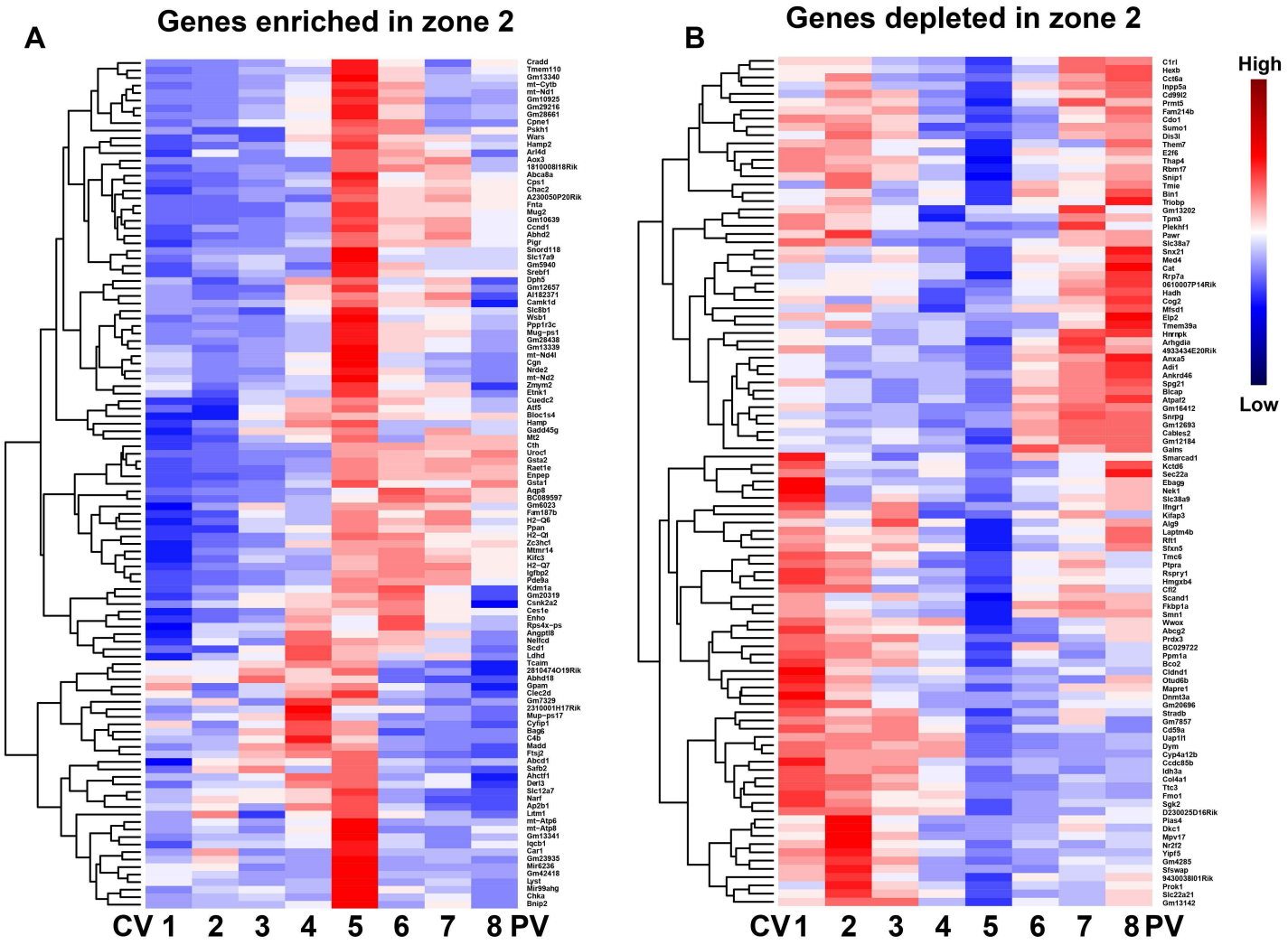

Fig. S13. Bulk transcriptomics from sorted zonal populations.

A. Bulk RNA-seq data from sorted zone-specific hepatocytes. Data was obtained from (*24*). The most upregulated genes in the midlobular regions of the lobule are shown in this heatmap. Groups 1-8 refer to sorted populations across the CV-PV axis, with group 1 being the closest to the CV and group 8 being the closest to the PV. The expression data associated with this figure is contained in Table S3.

B. The most downregulated genes in the midlobular regions of the lobule are shown in this heatmap.

Fig. S14.

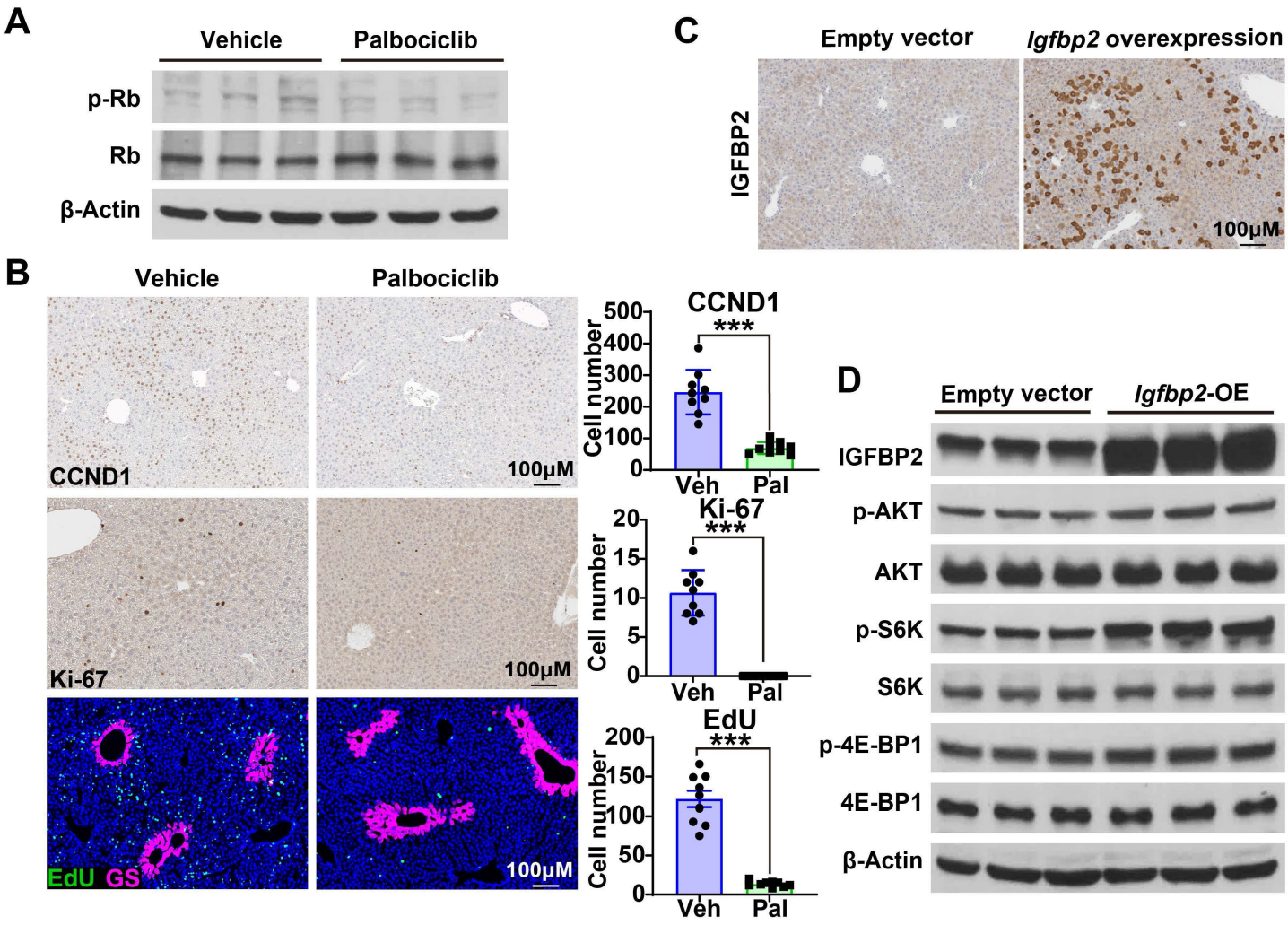

Fig. S14. Palbociclib administration leads to impaired zone 2 proliferation and overexpression of IGFBP2 causes mTOR pathway activation.

- **A.** 8 week old wild-type mice were treated with palbociclib, a CDK4/6-CCND1 complex inhibitor (n = 3, 3 mice treated with vehicle or drug). Two days after palbociclib initiation, EdU water was provided for 10 days. Western blot analysis from harvested livers is shown.
- **B.** IHC showing CCND1 and Ki-67 along with IF showing EdU in livers of vehicle and palbociclib treated mice. Cell numbers for three image fields per mouse are quantified on the right.
- **C.** IHC showing IGFBP2 overexpression 48 hours after HDT injection of a transposon containing the *Igfbp2* cDNA in wild-type livers (n = 3, 3 mice).
- **D.** AKT-mTOR pathway components assessed by western blot analysis.

Fig. S15.

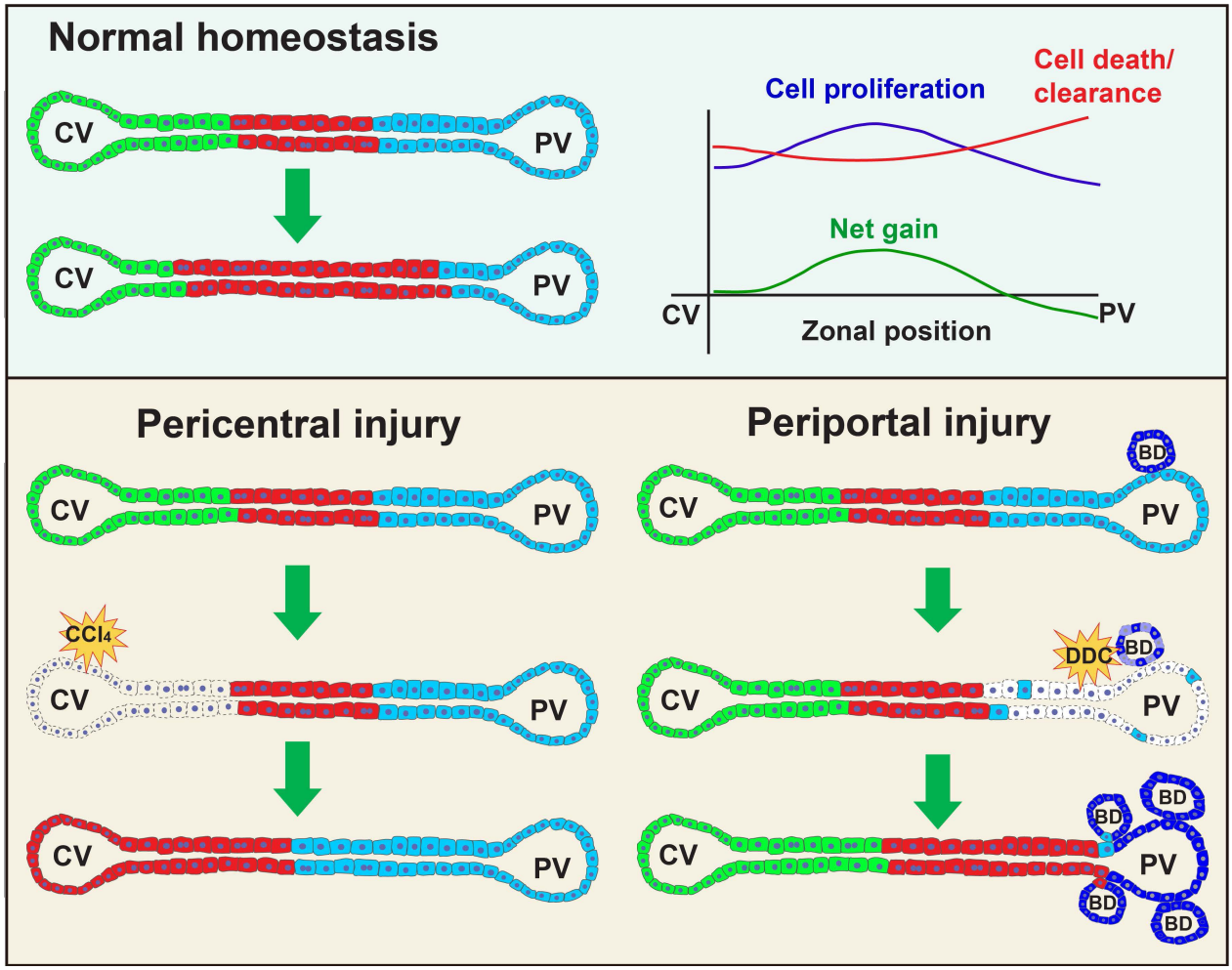

Fig. S15. Model for zone 2 hepatocyte repopulation during normal homeostasis and regeneration after injury.

Table S1.
CRISPR knock-in mouse reagents and success rates.
For all lines, we used CRISPR methodology to integrate an IRES cassette followed by *CreER* into the endogenous 3'UTRs of genes with zone specific expression patterns. This table contains two separate excel sheets. Sheet 1 contains the types of reagents used, the homology arm lengths, and microinjection results from the live pups delivered from the CRI Mouse Genome Engineering Core. "CreER positive" refers to the number of randomly integrated mice and correctly knocked-in mice. Sheet 2 shows the primer sequences used to genotype knock-in integration sites. These primers were used to determine the presence of the *CreER* and to distinguish between distinct *CreER* integrations. For all genotyping, both L and R primer pairs are used to confirm the correct *CreER* strain. See Fig. S1B-K for the appearance of genotyping bands on DNA gels.

Table S2.
Differentially expressed genes from liver scRNA-seq analysis.
Sheet 1: The most differentially expressed genes in each of the three zones, z-score data associated with Fig. S12G.
Sheet 2: Differentially expressed genes in zone 1 compared to all hepatocytes.
Sheet 3: Differentially expressed genes in zone 2 compared to all hepatocytes.
Sheet 4: Differentially expressed genes in zone 3 compared to all hepatocytes.
Sheet 5: Differentially expressed genes in Hamp2 expressing hepatocytes vs. all hepatocytes.
Sheet 6: Differentially expressed genes in GS expressing hepatocytes vs. all hepatocytes.
Sheet 7: Differentially expressed genes in Sox9 expressing hepatocytes vs. all hepatocytes.

Table S3.
Bulk RNA-seq data from sorted zonal populations in the liver.
This data was obtained from (*24*). Groups 1-8 in these excel spreadsheets refer to sorted populations across the CV-PV axis, with group 1 being the closest to the CV and group 8 being the closest to the PV. The expression heatmaps are shown in Fig. S13. 176 of these 216 genes that have associated CRISPR KO and CRISPRa sgRNAs were included in the in vivo CRISPR screens.
Sheet 1: 113 upregulated genes within zone 2 as compared to zones 1 and 3.
Sheet 2: 103 downregulated genes within zone 2 as compared to zones 1 and 3.

Table S4.
In vivo CRISPR screening data.
Sheet 1: CRISPR KO sgRNAs for 176 genes and controls were extracted from the Mouse CRISPR Knockout Pooled Library (GeCKO v2) (Addgene #1000000052).
Sheet 2: Results for the CRISPR KO screen.
Sheet 3: CRISPRa sgRNAs for 175 genes and controls were extracted from the Mouse Genome-wide CRISPRa-v2 Library (Addgene #83996).
Sheet 4: Results for the CRISPRa screen.
Sheet 5: Genes that are overlapping in the screens. For both screens we used a p-value cutoff of < 0.15 to select genes of interest.

References and Notes

1. L. Kulik, H. B. El-Serag, Epidemiology and management of hepatocellular carcinoma. *Gastroenterology* **156**, 477–491.e1 (2019). doi:10.1053/j.gastro.2018.08.065 Medline

2. J. Font-Burgada, S. Shalapour, S. Ramaswamy, B. Hsueh, D. Rossell, A. Umemura, K. Taniguchi, H. Nakagawa, M. A. Valasek, L. Ye, J. L. Kopp, M. Sander, H. Carter, K. Deisseroth, I. M. Verma, M. Karin, Hybrid periportal hepatocytes regenerate the injured liver without giving rise to cancer. *Cell* **162**, 766–779 (2015). doi:10.1016/j.cell.2015.07.026 Medline

3. B. Wang, L. Zhao, M. Fish, C. Y. Logan, R. Nusse, Self-renewing diploid Axin2$^+$ cells fuel homeostatic renewal of the liver. *Nature* **524**, 180–185 (2015). doi:10.1038/nature14863 Medline

4. S. Lin, E. M. Nascimento, C. R. Gajera, L. Chen, P. Neuhöfer, A. Garbuzov, S. Wang, S. E. Artandi, Distributed hepatocytes expressing telomerase repopulate the liver in homeostasis and injury. *Nature* **556**, 244–248 (2018). doi:10.1038/s41586-018-0004-7 Medline

5. W. Pu, H. Zhang, X. Huang, X. Tian, L. He, Y. Wang, L. Zhang, Q. Liu, Y. Li, Y. Li, H. Zhao, K. Liu, J. Lu, Y. Zhou, P. Huang, Y. Nie, Y. Yan, L. Hui, K. O. Lui, B. Zhou, Mfsd2a$^+$ hepatocytes repopulate the liver during injury and regeneration. *Nat. Commun.* **7**, 13369 (2016). doi:10.1038/ncomms13369 Medline

6. K. Furuyama, Y. Kawaguchi, H. Akiyama, M. Horiguchi, S. Kodama, T. Kuhara, S. Hosokawa, A. Elbahrawy, T. Soeda, M. Koizumi, T. Masui, M. Kawaguchi, K. Takaori, R. Doi, E. Nishi, R. Kakinoki, J. M. Deng, R. R. Behringer, T. Nakamura, S. Uemoto, Continuous cell supply from a Sox9-expressing progenitor zone in adult liver, exocrine pancreas and intestine. *Nat. Genet.* **43**, 34–41 (2011). doi:10.1038/ng.722 Medline

7. Y. Malato, S. Naqvi, N. Schürmann, R. Ng, B. Wang, J. Zape, M. A. Kay, D. Grimm, H. Willenbring, Fate tracing of mature hepatocytes in mouse liver homeostasis and regeneration. *J. Clin. Invest.* **121**, 4850–4860 (2011). doi:10.1172/JCI59261 Medline

8. K. Yanger, D. Knigin, Y. Zong, L. Maggs, G. Gu, H. Akiyama, E. Pikarsky, B. Z. Stanger, Adult hepatocytes are generated by self-duplication rather than stem cell differentiation. *Cell Stem Cell* **15**, 340–349 (2014). doi:10.1016/j.stem.2014.06.003 Medline

9. T. Sun, M. Pikiolek, V. Orsini, S. Bergling, S. Holwerda, L. Morelli, P. S. Hoppe, L. Planas-Paz, Y. Yang, H. Ruffner, T. Bouwmeester, F. Lohmann, L. M. Terracciano, G. Roma, F. Cong, J. S. Tchorz, AXIN2$^+$ pericentral hepatocytes have limited contributions to liver homeostasis and regeneration. *Cell Stem Cell* **26**, 97–107.e6 (2020). doi:10.1016/j.stem.2019.10.011 Medline

10. F. Chen, R. J. Jimenez, K. Sharma, H. Y. Luu, B. Y. Hsu, A. Ravindranathan, B. A. Stohr, H. Willenbring, Broad distribution of hepatocyte proliferation in liver homeostasis and regeneration. *Cell Stem Cell* **26**, 27–33.e4 (2020). doi:10.1016/j.stem.2019.11.001 Medline

11. W. Birchmeier, Orchestrating Wnt signalling for metabolic liver zonation. *Nat. Cell Biol.* **18**, 463–465 (2016). doi:10.1038/ncb3349 Medline

12. S. Ben-Moshe, S. Itzkovitz, Spatial heterogeneity in the mammalian liver. *Nat. Rev. Gastroenterol. Hepatol.* **16**, 395–410 (2019). doi:10.1038/s41575-019-0134-x Medline

13. S. A. MacParland, J. C. Liu, X.-Z. Ma, B. T. Innes, A. M. Bartczak, B. K. Gage, J. Manuel, N. Khuu, J. Echeverri, I. Linares, R. Gupta, M. L. Cheng, L. Y. Liu, D. Camat, S. W. Chung, R. K. Seliga, Z. Shao, E. Lee, S. Ogawa, M. Ogawa, M. D. Wilson, J. E. Fish, M. Selzner, A. Ghanekar, D. Grant, P. Greig, G. Sapisochin, N. Selzner, N. Winegarden, O. Adeyi, G. Keller, G. D. Bader, I. D. McGilvray, Single cell RNA sequencing of human liver reveals distinct intrahepatic macrophage populations. *Nat. Commun.* **9**, 4383 (2018). doi:10.1038/s41467-018-06318-7 Medline

14. K. B. Halpern, R. Shenhav, O. Matcovitch-Natan, B. Tóth, D. Lemze, M. Golan, E. E. Massasa, S. Baydatch, S. Landen, A. E. Moor, A. Brandis, A. Giladi, A. S. Avihail, E. David, I. Amit, S. Itzkovitz, Single-cell spatial reconstruction reveals global division of labour in the mammalian liver. *Nature* **542**, 352–356 (2017). doi:10.1038/nature21065 Medline

15. N. Aizarani, A. Saviano, L. Sagar, L. Mailly, S. Durand, J. S. Herman, P. Pessaux, T. F. Baumert, D. Grün, A human liver cell atlas reveals heterogeneity and epithelial progenitors. *Nature* **572**, 199–204 (2019). doi:10.1038/s41586-019-1373-2 Medline

16. A. L. Means, Y. Xu, A. Zhao, K. C. Ray, G. Gu, A CK19^{CreERT} knockin mouse line allows for conditional DNA recombination in epithelial cells in multiple endodermal organs. *Genesis* **46**, 318–323 (2008). doi:10.1002/dvg.20397 Medline

17. S. Ghafoory, K. Breitkopf-Heinlein, Q. Li, C. Scholl, S. Dooley, S. Wölfl, Zonation of nitrogen and glucose metabolism gene expression upon acute liver damage in mouse. *PLOS ONE* **8**, e78262 (2013). doi:10.1371/journal.pone.0078262 Medline

18. A. Raven, W.-Y. Lu, T. Y. Man, S. Ferreira-Gonzalez, E. O'Duibhir, B. J. Dwyer, J. P. Thomson, R. R. Meehan, R. Bogorad, V. Koteliansky, Y. Kotelevtsev, C. Ffrench-Constant, L. Boulter, S. J. Forbes, Cholangiocytes act as facultative liver stem cells during impaired hepatocyte regeneration. *Nature* **547**, 350–354 (2017). doi:10.1038/nature23015 Medline

19. X. Deng, X. Zhang, W. Li, R.-X. Feng, L. Li, G.-R. Yi, X.-N. Zhang, C. Yin, H.-Y. Yu, J.-P. Zhang, B. Lu, L. Hui, W.-F. Xie, Chronic liver injury induces conversion of biliary epithelial cells into hepatocytes. *Cell Stem Cell* **23**, 114–122.e3 (2018). doi:10.1016/j.stem.2018.05.022 Medline

20. T.-Y. Choi, N. Ninov, D. Y. R. Stainier, D. Shin, Extensive conversion of hepatic biliary epithelial cells to hepatocytes after near total loss of hepatocytes in zebrafish. *Gastroenterology* **146**, 776–788 (2014). doi:10.1053/j.gastro.2013.10.019 Medline

21. P. Bergmann, K. Militzer, P. Schmidt, D. Büttner, Sex differences in age development of a mouse inbred strain: Body composition, adipocyte size and organ weights of liver, heart and muscles. *Lab. Anim.* **29**, 102–109 (1995). doi:10.1258/002367795780740447 Medline

22. P. Fickert, U. Stöger, A. Fuchsbichler, T. Moustafa, H.-U. Marschall, A. H. Weiglein, O. Tsybrovskyy, H. Jaeschke, K. Zatloukal, H. Denk, M. Trauner, A new xenobiotic-

induced mouse model of sclerosing cholangitis and biliary fibrosis. *Am. J. Pathol.* **171**, 525–536 (2007). doi:10.2353/ajpath.2007.061133 Medline

23. B. D. Tarlow, M. J. Finegold, M. Grompe, Clonal tracing of $Sox9^+$ liver progenitors in mouse oval cell injury. *Hepatology* **60**, 278–289 (2014). doi:10.1002/hep.27084 Medline

24. S. Ben-Moshe, Y. Shapira, A. E. Moor, R. Manco, T. Veg, K. Bahar Halpern, S. Itzkovitz, Spatial sorting enables comprehensive characterization of liver zonation. *Nat. Metab.* **1**, 899–911 (2019). doi:10.1038/s42255-019-0109-9 Medline

25. M. Zhu, T. Lu, Y. Jia, X. Luo, P. Gopal, L. Li, M. Odewole, V. Renteria, A. G. Singal, Y. Jang, K. Ge, S. C. Wang, M. Sorouri, J. R. Parekh, M. P. MacConmara, A. C. Yopp, T. Wang, H. Zhu, Somatic mutations increase hepatic clonal fitness and regeneration in chronic liver disease. *Cell* **177**, 608–621.e12 (2019). doi:10.1016/j.cell.2019.03.026 Medline

26. C. Espeillac, C. Mitchell, S. Celton-Morizur, C. Chauvin, V. Koka, C. Gillet, J. H. Albrecht, C. Desdouets, M. Pende, S6 kinase 1 is required for rapamycin-sensitive liver proliferation after mouse hepatectomy. *J. Clin. Invest.* **121**, 2821–2832 (2011). doi:10.1172/JCI44203 Medline

27. L. Planas-Paz, V. Orsini, L. Boulter, D. Calabrese, M. Pikiolek, F. Nigsch, Y. Xie, G. Roma, A. Donovan, P. Marti, N. Beckmann, M. T. Dill, W. Carbone, S. Bergling, A. Isken, M. Mueller, B. Kinzel, Y. Yang, X. Mao, T. B. Nicholson, R. Zamponi, P. Capodieci, R. Valdez, D. Rivera, A. Loew, C. Ukomadu, L. M. Terracciano, T. Bouwmeester, F. Cong, M. H. Heim, S. J. Forbes, H. Ruffner, J. S. Tchorz, The RSPO-LGR4/5-ZNRF3/RNF43 module controls liver zonation and size. *Nat. Cell Biol.* **18**, 467–479 (2016). doi:10.1038/ncb3337 Medline

28. C. H. Ang, S. H. Hsu, F. Guo, C. T. Tan, V. C. Yu, J. E. Visvader, P. K. H. Chow, N. Y. Fu, $Lgr5^+$ pericentral hepatocytes are self-maintained in normal liver regeneration and susceptible to hepatocarcinogenesis. *Proc. Natl. Acad. Sci. U.S.A.* **116**, 19530–19540 (2019). doi:10.1073/pnas.1908099116 Medline

29. S. Tanami, S. Ben-Moshe, A. Elkayam, A. Mayo, K. Bahar Halpern, S. Itzkovitz, Dynamic zonation of liver polyploidy. *Cell Tissue Res.* **368**, 405–410 (2017). doi:10.1007/s00441-016-2427-5 Medline

30. A. Benedetti, A. M. Jézéquel, F. Orlandi, Preferential distribution of apoptotic bodies in acinar zone 3 of normal human and rat liver. *J. Hepatol.* **7**, 319–324 (1988). doi:10.1016/S0168-8278(88)80004-7 Medline

31. A. Benedetti, A. M. Jezequel, F. Orlandi, A quantitative evaluation of apoptotic bodies in rat liver. *Liver* **8**, 172–177 (1988). doi:10.1111/j.1600-0676.1988.tb00987.x Medline

32. X. Sun, J.-C. Chuang, M. Kanchwala, L. Wu, C. Celen, L. Li, H. Liang, S. Zhang, T. Maples, L. H. Nguyen, S. C. Wang, R. A. J. Signer, M. Sorouri, I. Nassour, X. Liu, J. Xu, M. Wu, Y. Zhao, Y.-C. Kuo, Z. Wang, C. Xing, H. Zhu, Suppression of the SWI/SNF component *Arid1a* promotes mammalian regeneration. *Cell Stem Cell* **18**, 456–466 (2016). doi:10.1016/j.stem.2016.03.001 Medline

33. A. N. Bowman, R. van Amerongen, T. D. Palmer, R. Nusse, Lineage tracing with Axin2 reveals distinct developmental and adult populations of Wnt/β-catenin–responsive neural

stem cells. *Proc. Natl. Acad. Sci. U.S.A.* **110**, 7324–7329 (2013). doi:10.1073/pnas.1305411110 Medline

34. R. van Amerongen, A. N. Bowman, R. Nusse, Developmental stage and time dictate the fate of Wnt/β-catenin-responsive stem cells in the mammary gland. *Cell Stem Cell* **11**, 387–400 (2012). doi:10.1016/j.stem.2012.05.023 Medline

35. J. L. Kopp, C. L. Dubois, A. E. Schaffer, E. Hao, H. P. Shih, P. A. Seymour, J. Ma, M. Sander, Sox9^{+} ductal cells are multipotent progenitors throughout development but do not produce new endocrine cells in the normal or injured adult pancreas. *Development* **138**, 653–665 (2011). doi:10.1242/dev.056499 Medline

36. H. Zhu, S. Shah, N. Shyh-Chang, G. Shinoda, W. S. Einhorn, S. R. Viswanathan, A. Takeuchi, C. Grasemann, J. L. Rinn, M. F. Lopez, J. N. Hirschhorn, M. R. Palmert, G. Q. Daley, *Lin28a* transgenic mice manifest size and puberty phenotypes identified in human genetic association studies. *Nat. Genet.* **42**, 626–630 (2010). doi:10.1038/ng.593 Medline

37. W.-C. Li, K. L. Ralphs, D. Tosh, Isolation and culture of adult mouse hepatocytes. *Methods Mol. Biol.* **633**, 185–196 (2010). doi:10.1007/978-1-59745-019-5_13 Medline

38. F. A. Wolf, P. Angerer, F. J. Theis, SCANPY: Large-scale single-cell gene expression data analysis. *Genome Biol.* **19**, 15 (2018). doi:10.1186/s13059-017-1382-0 Medline

39. L. Haghverdi, A. T. L. Lun, M. D. Morgan, J. C. Marioni, Batch effects in single-cell RNA-sequencing data are corrected by matching mutual nearest neighbors. *Nat. Biotechnol.* **36**, 421–427 (2018). doi:10.1038/nbt.4091 Medline

40. V. A. Traag, L. Waltman, N. J. van Eck, From Louvain to Leiden: Guaranteeing well-connected communities. *Sci. Rep.* **9**, 5233 (2019). doi:10.1038/s41598-019-41695-z Medline

41. V. D. Blondel, J.-L. Guillaume, R. Lambiotte, E. Lefebvre, Fast unfolding of communities in large networks. *J. Stat. Mech.* **2008**, P10008 (2008). doi:10.1088/1742-5468/2008/10/P10008

42. M. C. Canver, M. Haeussler, D. E. Bauer, S. H. Orkin, N. E. Sanjana, O. Shalem, G.-C. Yuan, F. Zhang, J.-P. Concordet, L. Pinello, Integrated design, execution, and analysis of arrayed and pooled CRISPR genome-editing experiments. *Nat. Protoc.* **13**, 946–986 (2018). doi:10.1038/nprot.2018.005 Medline